DRAL
Daresbury Laboratory
Rutherford Appleton Laboratory

RAL Report
RAL-94-114

The Experimental Characterisation of Gas Microstrip Detectors III. Lifetime Characteristics

J E Bateman J F Connolly et al

November 1994

Rutherford Appleton Laboratory Chilton DIDCOT Oxfordshire OX11 0QX

RAL-94-114

THE EXPERIMENTAL CHARACTERISATION OF GAS MICROSTRIP DETECTORS

III. LIFETIME CHARACTERISTICS

J E Bateman and J F Connolly
Rutherford Appleton Laboratory, Chilton, Didcot, OX11 0QX, U.K.

Yu N Pestov and L I Shekhtman
Budker Institute of Nuclear Physics, 630090 Novosibirsk, Russia

R Mutikainen and I Suni
VTT Electronics, P O Box 1101, 02044VTT, Espoo, Finland

The results of a programme of research into the experimental properties of gas microstrip detectors are reported. In this report information on the lifetime characteristics of the devices is presented.

1. INTRODUCTION

Since its introduction by Oed [1], the gas microstrip detector (GMSD) has been studied by several groups for potential applications in high energy physics, space science, materials science and medicine.[2-8] The GMSD is a form of the gas proportional counter in which an extremely precise pattern of metallisation is laid down on an insulating substrate using standard microlithographic techniques. The pattern consists of interleaved narrow (typically 10μm) and wide (typically 100μm) metal strips separated by (typically) around 100μm strips of insulating substrate. Application of a few hundred volts between the anode and cathode strips in a suitable gas atmosphere results in amplification factors of up to 10000 for any free electrons captured by the anode. Figure 1 shows a typical detector structure with a drift electrode spaced a few millimeters away from the lithographic plate to define the active volume of the detector.

As a potential replacement for the multiwire proportional counter (MWPC) the GMSD has several attractions. First, independent detectors can be made on a pitch of 0.25mm or less; second, the positional accuracy of the electrodes essential for all gas detectors can be achieved easily and without the demand for structural strength which wire tensions impose on the MWPC; third, the very small anode-cathode gap leads to sub-microsecond positive ion transit times thus permitting count rate densities two orders of magnitude higher than is possible with a wire counter. The excellent spatial resolution ($<30\mu$m) has been demonstrated in high energy particle tracking [3] and the structural precision has permitted excellent energy resolution [5].

The undoubted potential of the GMSD was vitiated throughout its early development by the presence of gain instabilities which are severely aggravated by high counting rates so robbing it of its one great advantage over a wire counter. This gain instability was quickly determined to be a result of the effect of the very high electric fields at the edge of the anode on the substrate material. In extensive tests with conventional glasses (pyrex, etc) [9] the well-known ionic polarisation effects of such materials were shown to be responsible. When it was suggested [10,11] that semiconducting glasses might offer a more stable substrate we immediately obtained samples and produced GMSDs on them. The resulting detectors showed a degree of stability and reproducibility which, for the first time, made systematic measurements on our GMSDs possible.

The investigations performed at RAL into the gain and rate characteristics of GMSDs fabricated on semiconducting glasses have been reported elsewhere [12,13]. In the course of this work it became apparent that while the short term ageing effects observed with ionically conducting glass substrates (e.g. pyrex glass) had disappeared, permanent deterioration of the gain was occurring at accumulated signal charge values of a fraction of a millicoulomb/cm of anode strip. Such a short lifetime would preclude the application of GMSDs in most of the potential applications foreseen. We therefore commenced a programme to explore the implications for GMSD lifetimes of some configurations of detector and gas systems.

2. AGEING OF GAS DETECTORS

The deterioration of gas detectors as a result of the avalanche process is well documented and is the subject of a comprehensive review by Kadyk [14]. The damage to the counters is usually observed as deposits on either (or both) anode and cathode surfaces. The former tends to lead to sparking and the latter to increased noise in the long term. When the common gas mixtures with hydrocarbon quenchers are used, the deposits can usually be identified as polymeric forms of the quencher. A common interpretation of the loss of gain observed in a wire counter is that the deposits increase the effective anode wire diameter and so reduce the amplifying electric field. In the GMSD we have the added complication that chemically active ions released in the avalanche can attach themselves to the substrate adjacent to the anode (and cathode) edge and by modifying the conductivity of the surface also modulate the gain of the detector both upwards and downwards [9]. As we shall see, GMSDs (unlike wire counters) can exhibit a positive ageing coefficient.

The formation of avalanche-induced deposits is a chemical process which can be catalysed both by the substrate itself and by trace impurities (e.g. halogens) in the gas. Thus it is clear that the lifetime of a GMSD can be affected by every significant parameter in its manufacture and operation: substrate, metallisation, processing, gas composition, gas purity, etc. and one must make the best guesses one can in the search for a configuration which will yield a significant improvement in the lifetime. Following the promising ageing results from CERN [15] we elected to study the combination of our semiconducting plates with a clean argon/dimethylether (DME) gas mixture. For reference some studies with argon/isobutane were also performed.

3. THE CONDITIONS OF THE TESTS

3.1 The Detectors

Test detectors were fabricated using the basic pattern of figure 1. In the lithography 20 anodes (60mm long) are bussed together with a connecting pad at the outboard end and the corresponding cathodes are similarly treated. This results in an active detector area of 6mm x 60mm with this pattern repeated five times on a standard 100mm x100mm glass plate giving five independent detectors. Three plates were used in the present tests:

#202: Pestov glass of 10^9 Ω-cm (P9) metallised with a triple process in which the pattern is formed on thin titanium and nickel layers and is then plated up with gold to a thickness of $\approx 0.5\mu$m. This was fabricated at Novosibirsk by a collaboration of Budker INP and NPO Vostok.

#206: Schott S8900 glass of 10^{11} Ω-cm metallised by a similar process to that of #202 with the seed layer for the gold being nickel (fabricated at VTT).

#207: Schott S8900 glass metallised with aluminium (0.5μm) by a conventional wet-etch process (fabricated at VTT).

The lithographic plates were supported on structures of standard glass-epoxy circuit boards, housed in an aluminium box with a rubber seal and an aluminised melinex window (50μm) for xray access. Electrical leadthroughs were made from standard SHV connectors sealed with epoxy.

3.2 The Gas System

The gas system was plumbed entirely in 6mm stainless steel tubing which had been thoroughly washed and dried before installation. Flexible stainless steel sections were used for connection to the detectors. The gas rig was kept as simple as possible with the gas bottles feeding (via regulators) two Brookes mass flowmeters before mixing in a manifold and distribution to the counters. No chemical filters or float-flowmeters were fitted. The Brookes flowmeter controlling the DME operated with its original Viton seal throughout.

The gases used were:

argon: standard research grade
DME1: standard commercial grade from BOC
DME2: standard commercial grade from Gerling-Holz
IB: standard commercial grade

The strong electronegative effects of impurities (oxygen ?) in DME provides a ready diagnostic for gas purity. Figure 2 shows the effect of impure gas on the pulse height resolution measured for the Cu xray peak when the system is inadequately outgassed (a) and when an inferior quality of DME (DME1) is used (b).

3.3 GMSD Operating Conditions

The operating potentials used in our tests were generally Va=0V, Vc=-600V to -800V and Vd= -2200V (figure 1). In order to achieve gas gains of $\approx$1000 (particularly with the P9 glass) it was necessary to make use of the "robber bar" electrode [12] which was run at $\approx$-1200V. As noted elsewhere [12] back electrodes are not appropriate for GMSDs fabricated on low-resistivity glass.

3.4 The Readout Electronics

The calibration of the charge dose to the GMSD depended on counting pulses. An Ortec 109PC charge preamplifier connected to an Ortec 460 Delay Line Shaping Amplifier enabled pulse rates of up to 500kHz to be observed with an individual pulse amplitude of 2.5 10^5 electrons. Errors due to electronic rate effects were avoided by the use of a calibrated attenuator foil for the xray beam (x28.2) which reduced rates to the domain in which deadtime corrections were negligible ($<$50kHz). The gain of the GMSD was measured by means of the xray peak position in a pulse height analyser (PHA) calibrated by a standard charge pulse injected into the preamplifier. In general this measurement was carried out with the attenuating foil in place in order to make the rate acceptable to the PHA. The inevitable gain deficit arising from the extremely high flux density of events (up to 500kHz/mm^2)could

be observed on a CRT attached to the output of the main amplifier and the approriate correction factor (≈ 0.75 in the case of a P9 plate at 500kHz/mm^2) applied to the charge dose calculation).

3.5 The Test Beam

The xray test beam was supplied by a copper anode generator set via a brass collimator of aperture 0.9mm diameter with a 2 degree crossfire angle. Positioned within 5mm of the drift electrode of the GMSD, the area of impact on the plate was estimated to be ≈ 1mm^2. Since the plate pattern has a repeat pitch of 0.3mm this corresponded to 3.3mm of anode length. The charge dose to the plate could thus be estimated as the product of: counting rate * pulse height * 3 coulombs/cm.

3.6 Control of Ambient Variables

The magnitude of the anticipated gain shift induced by ageing was susceptible to being masked (or confused) by the gain shifts induced in a flow-gas counter by changes in the ambient variables, pressure (P) and temperature (T). Using the model for the gain of a gas counter suggested by Bateman [16] it is easy to show that the relative gain coefficient 1/GdG/dq (where G is the gas gain and q is the variable P/T) is essentially independent of the gain (over a reasonable range of gain). Thus it is possible to evaluate this coefficient over a few days in advance of a long exposure and use it to remove ambient effects from the raw data as long as P and T are recorded for each gain measurement. In the case of the low resistivity Pestov glass a further complication arises due to the temperature dependence of the large leakage current ($\approx 25\mu$A) and the corresponding bias changes induced by the protection resistor (2.3MΩ). This complication was removed by taking the gain measurement as the ambient temperature passed through a standard value once per day.

3.7 The Test Procedure

Having performed the various calibration procedures noted above, exposure on a part of the plate was initiated, the rate being set around 500kHz. Close monitoring followed to see if this rate could be supported by the plate. If sparking occurred the rate was reduced and monitoring continued until stable operation was obtained. All lifetime exposures were done at the maximum possible rate permitting stable operation.

The attenuated beam was now moved to a fresh area of the counter and the gain scanned across the intended operating site for 10mm either side in X (along the strips) and across the 6mm width of the detector in Y. In a few cases a complete bidimensional scan of the area around the site (at 1mm intervals) was performed. These measurements formed the reference for gain shifts induced by irradiation.

Irradiation was then commenced at the chosen rate. At intervals (initially every few minutes and later every hour or two) the attenuator foil was inserted and the xray peak channel and full width at half maximum (FWHM) recorded along with P,T, the leakage current, the

elapsed time and the rate. For the first two days exposure was only applied during working hours so that any early failure could be observed. After confidence had been established the exposure was continuous except for the minute or so required for the gain measurement. Gain scans (which required around 30 minutes to complete) were performed every two days during long runs.

4.0 RESULTS

4.1 Pestov Glass (Plate #202 - Au/Ni/Ti metallisation)

Figure 3 shows the relative gain observed at one irradiation site on plate #202 in an argon/DME gas mixture (unless otherwise stated the DME used is from the Gerling-Holz batch) throughout a period of 261 hours when it was exposed to a continuous rate of 500kHz/mm^2 with a gas gain of $\approx$800. No sparking or instability of any kind was observred during this period. For comparison the gain plot of an exposure of a different site of the same plate running in an argon/isobutane gas mixture is shown. The maximum rate which this configuration would tolerate without sparking was 160kHz at a gas gain of $\approx$1000. The detector ran with no visible sign of distress for around 19 hours when intermittent sparking developed. From this point on the gain began to decrease rapidly and at 21 hours the sparking was so severe that the exposure was discontinued. Thus while the argon/DME run showed stable behavior up to 40mC/cm (aggregate charge delivered to 1cm of anode strip) with every indication that it could continue much further, the argon/isobutane run ended in terminal damage at $\approx$1mC/cm.

Figure 4 shows the relative gain plots of two separate irradiation sites on plate #202 when taken to an accumulated charge dose of 40mC/cm in an argon/DME gas mixture with gains of 900 and 800 respectively at 500kHz. While not identical, the two curves are consistent in showing a gain rise of $\approx$6% followed by a decline, the original gain not being reached by 40mC/cm. As figure 5 shows the situation is not as simple as figure 4 seems to imply. A scan of the gain across the irradiation site shows that the response function of the plate to the beam is a central peak with negative tails which spread out to a radial distance of at least 10mm from the beam site. When, after $\approx$40mC/cm the gain under the beam has returned to approximately the starting value, there is a deficit of somewhat less than 10% in a ring around the edge of the beam. The central peak is clearly seen in figure 6 which shows a bidimensional gain scan after irradiation, normalised to one made just before the exposure. The contours are in 1% steps. The normalisation of the peak to 97% (instead of 100.5% as figure 4 indicates) arises simply because the P/T effects have not been normalised out in this plot.

When serious damage occurs to a GMSD one of the first parameters to suffer is usually the FWHM of the xray peak. (For example, after an hour of intermittent sparking in argon/isobutane the FWHM had doubled and was deteriorating rapidly.) Figure 7 shows a plot of the FWHM across the irradiated area of figure 5 (i.e. after the full 40mC/cm). There is absolutely no sign of any deterioration from the pristine value of 11% anywhere across the plate.

4.2 Schott S8900 glass (Plate #206 - Au/Ni metallisation)

The ageing procedures described above for the Pestov glass GMSDs were repeated for the plates fabricated on S8900 glass. The correction for P/T effects was rendered much simpler due to the negligible effect of the leakage current ($\approx 0.3\mu A$) on the gain variations. While a gain of ≈ 1000 could easily be attained the maximum rate tolerated by these plates in argon/DME was 300kHz. This increased the period of exposure required to achieve 40mC/cm to around one month.

Figure 8 shows the relative gain plot observed on plate #206 for the beam spot over this exposure (initial gain=957, argon +17%DME). The behaviour is similar to that of plate #202 but the initial rise in the gain ($\approx 5\%$) occurs much sooner and the subsequent decline leads to a deficit of 11% after 46mC/cm. Figure 9 shows this data plotted with the dose on a logarithmic scale. Here the rise and fall are clearer and it appears that in the region of gain decline the gain can be fitted to a function of the form g = a - b*ln(x) where g is the gain, x the charge dose and a and b are constants. Since the counter is perfectly stable at the 46mC/cm mark we may risk using the fit to extrapolate to a dose of 100mC/cm where a deficit of 15% is predicted.

The spatial distribution of the gain excursion generated by the beam (46mC/cm) is different from that observed on plate #202 with a simple dip around the beam spot limited to a radius of about 2mm. The magnitude of the effect (-11%) is, however, rather similar to that of the circular dip observed on #202 (figure 10).

The data of the periodic gain scans across the target area can be used to normalise out the P/T effects (the gain values at the extreme ends of the scan are assumed to be unaffected by the beam). Figure 11 shows a relative gain scan (with the elapsed time as the abscissa) for this exposure done in this way. This data also shows a logarithmic decline of the gain in agreement with figure 9.

Figure 12 shows the FWHM of the xray peak as a function of the charge dose during this exposure. Here we see a slow (logarithmic) deterioration from 12% to 16% at 46mC/cm. This stable curve again argues for the possibility of useful lifetimes out to the order of 100mC/cm.

While GMSDs made with S8900 plates are remarkably stable compared to any device made on ionic glasses, they are not totally immune from transient effects on the time scale (minutes) characteristic of ion movement in the glass. Figure 13 shows the gain measured on plate #206 when the 300kHz rate is applied to a fresh surface (upper curve) and removed from the site of prolonged irradiation (lower curve). The two excursions have approximately the same magnitude (5%) and time scales (30 minutes) but opposite signs. Given that they are reversible, they are unlikely to be due to deposits, but rather to some direct effect of the avalanches on the substrate conductivity mediated by either UV light or ions. The reversal of the sign is, on the other hand possibly attributable to a deposit.

The transients exhibited in figure 13 explain ragged data in the gain plots (figures 8,9). When the data was being logged, a short but indeterminate period of a few minutes would elapse between the insertion of the attenuator foil and the acquisition of the PHA data. Since this

corresponds to the time of greatest rate of change of the gain, an error of a percent or two was inevitable.

4.3 Schott S8900 glass (Plate #207 - Al metallisation)

The results of the attempt to reproduce the lifetime behaviour of plate #206 with plate #207 (Al metallisation) under similar conditions to those used above are shown in figure 14. With a gain of 1100, a rate of 150kHz and the same gas (argon + 17% DME) The gain of the plate declined steadily during the short run of 4 hours before the counter sparked and tripped the HV supply when a charge dose of 0.22mC/cm had been accumulated. Figure 14 shows the data for plate #206 for comparison.

4.4 Comparison of Plates #206 and #207 with CF4/DME Gas

Figure 15 shows a comparison between the Au/Ni and Al coated plates when run in a gas mixture of CF4 + 20% DME. The Au/Ni plate shows no significant gain loss at 1.2mC/cm whereas the Al plate has lost 20% of its gain at 0.1mC/cm

4.5 Visual Diagnostics

Inspection of the irradiation sites under the microscope provides further information on the ageing process. Inspection of plate #202 (Pestov glass) at the sites irradiated in an argon/isobutane atmosphere show intense semicircular black spots of a few microns diameter lining the edges of both the anode and cathode strips. In the cases in which sparking had commenced intense blackening covered an area equivalent to the beam diameter. The regions under the beam during the irradiation in an argon/DME atmosphere show a faint brown discoloration (of approximately twice the beam diameter) to the naked eye which is quite difficult to see under the microscope and a few small black spots appear at the electrode edges. There is no sign of the slightest damage to the metallisation in these areas after the dose of 40mC/cm.

The region of the 46mC/cm irradiation on plate #206 (S8900-Au/Ni) was photographed at VTT and figure 16 shows the result. The area of the beam core is clearly mapped out by the deposits present on the glass. A further notable feature is the discoloration of the electrodes by the deposits which is significantly more intense in the case of the anodes. On the glass the deposits extend to a radius of $\approx 500\mu$m (figure 16) but the electrode patterns show an interesting structure with the maximum deposit on the anodes being central, extending out to a radius of $\approx 750\mu$m and the cathode deposits being very low in the central 500μm, peaking at about 750μm and fading away out to $\approx 2500\mu$m. This ring structure is, in fact, visible to the naked eye. Figure 17 shows the contrast in deposits between the anode and cathode in the central region and figure 18 shows a magnified image of the deposits on the glass near the cathode edge.

4.6 Chemical analysis of the deposits

Chemical analysis of the deposits created on the surface of plate #206 by the extended irradiation was performed at VTT using ESCA (electron spectroscopy for chemical analysis) and FTIR (fourier transform infrared spectroscopy). The results were not conclusive, the most likely component being identified as probably a polyether.

5.DISCUSSION

Bearing in mind the caveat that ageing effects are chemical in origin and therefore subject to manifold subtleties, certain conclusions appear to emerge from our results:

(i) Gas mixtures with isobutane will not give a good lifetime. Our experience with methane is similar to that with isobutane and it seems reasonable to conclude that all hydrocarbons are unsuitable.

(ii) Aluminium metallisation (wet-etch) gives a very short lifetime while two-stage gold processes offer an excellent prospect for long lifetimes.

(iii) Our earlier work [12,13] showed that iron oxide-based semiconducting glasses of the "Pestov" type permit the fabrication of stable GMSDs. The present results indicate that both the P9 and the S8900 glasses give comparable lifetime behaviour.

(iv) While an ultra-clean gas system was used, the detector containment systems did not meet the same standard of hygiene. Outgassing effects were observed by means of the electron attachment effects in DME. We also found differences between sources of DME. However, the use of DME as the quencher did permit the realisation of useful detector lifetimes.

(v) Avalanche-induced ageing was observed with our most successful GMSDs which consisted of either P9 or S8900 glass plates processed with gold metallisation and operated in an argon +17%DME atmosphere supplied from a clean gas system. The effects of the ageing were observed as a modulation of the gain (initially upwards by a few % and later a steady logarithmic decrease amounting to -11% after a dose of 46mC/cm. A localised gain effect was noted which correlated with deposits observed on the anodes, cathodes and substrate. No damage to the electrodes was observed.

(vi) The ring structure observed in the gain modulation after intense irradiation (figure 5) (and also in the visually observed deposits) is almost certainly an artefact arising from the test conditions of intense flux. The positive ion flux returning to the drift cathode under these conditions distorts the drift field in such a way as to focus the electron clouds into a ring around the outside of the nominal beam diameter. Hence the most intense irradiation takes place in this ring and not under the centre of the x-ray beam. The appearance of deposits at distances of up to 10mm from the x-ray beam clearly indicates the importance of neutral (metastable) ions in the ageing process.

The level of lifetime performance achieved by our most successful system is possibly adequate for many applications. The constraints on window materials and the use of sealed

detectors over long periods may make it uneconomic to produce detector structures significantly more sanitary than the type we used. However, the work at CERN [15] indicates that with very clean conditions in the detector lifetimes extending beyond 100mC/cm are possible with negligible loss of gain. We shall investigate this possibility with new detector containment systems.

A close comparison of our experience with P9 and S8900 glass shows that the latter is preferable in respect of the low leakage current which it draws, however, given the use of a robber bar to prevent breakdown at the cathode ends, P9 permits significantly higher operating flux densities and also appears to exhibit smaller transient gain shifts. If P9 could be successfully operated as a thin film on an insulating substrate (as reported in [17]), the benefits of the low surface resistivity can be enjoyed without the excessive leakage currents. This is a technology that we hope to explore further at VTT and RAL.

At BNIP work continues on the development of a pulling process for the production of large area sheets of thin (0.3mm) semiconducting glass of 10^{11} Ω-cm, which would be suitable for high rate detectors in LHC applications.

REFERENCES

1. A Oed, Nucl Instr & Meth A263 (1988) 351-359

2. F Angelini, R Bellazzini, A Brez, M M Massai, G Spandre and M R Torquati, Nucl Instr & Meth A283 (1989) 755-761

3. F Angelini, R Bellazzini, A Brez, M M Massai, G Spandre, M R Torquati, R Bouclier, J Gauden and F Sauli, IEEE Trans Nuc Sci 37 (no.2) 1990 112

4. F Hartjes, B Hendriksen and F Udo, Nucl Instr & Meth A289 (1990) 384

5. C Butz-Jorgensen, Rev Sci Instrum 63 (1) 1992 648

6. J E Bateman, J F Connolly, R Stephenson and J Morse, Proceedings of the European Workshop on X-ray Detectors for Synchrotron Radiation Sources, Aussois, France 1991

7. L Alunni, R Bouclier, G Fara, Ch Garabatos, G Manzin, G Million, L Ropelewski, F Sauli, L I Shekhtman, E Daubie, O Pingot, Yu N Pestov, L Busso, and S Costa, Nucl Instr & Meth A348 (1994) 344-350

8. L I Shekhtman, High pressure gas avalanche chambers for medical radiology, presented at the Fourth International Conference on Application of Physics in Medicine and Biology, Trieste, 1992

9. J E Bateman and J F Connolly, Substrate-induced instability in gas microstrip detectors. RAL-92-085

10. G D Minakov, Yu N Pestov, V S Prokopenko and L I Shekhtman, Nucl Instr & Meth A326 (1993) 566-569

11. R Bouclier, G Million, L Ropelewski, F Sauli, Yu N Pestov and L I Shekhtman, Nucl Instr & Meth A332 (1993) 100-106

12. J E Bateman and J F Connolly, The experimental characterisation of gas microstrip detectors I. Gain characteristics RAL-93-090

13. J E Bateman and J F Connolly, The experimental characterisation of gas microstrip detectors II. Counting rate characteristics RAL-93-096

14. J A Kadyk, Nucl Instr & Meth A300 (1991) 436-479

15. R Bouclier, C Garabatos, G Manzin, G Million, F Sauli, T Temmel and L Shekhtman, Ageing studies with microstrip gas chambers, CERN-PPE/94-63

16. J E Bateman, Practical gain formulae for proportional counters, RAL-93-019

17. W G Gong, J W Harris and H Wieman, LBL - 35779 UC - 414

FIGURE CAPTIONS

Figure 1
A schematic section of the gas microstrip detector used throughout the studies reported in this paper.

Figure 2
This shows how the FWHM of the xray pulse height spectrum may be used to check gas purity in argon/DME gas mixtures. The plot of FWHM against the drift potential is compared in the cases: (a) Immediately on commissioning of the gas system and after three weeks of purging and (b) When two different supplies of DME are used. With impure gas there is a drastic degradation of the FWHM at low drift fields due to electron attachment.

Figure 3
The relative gas gain behaviour under avalanche loading as observed on plate #202 (P9 glass-Au/Ni/Ti processing) for an argon + 10% isobutane mixture and an argon + 17% DME mixture.

Figure 4
The gas gain behaviour at two separate locations on plate #202 when subjected to continuous exposure up to 40mC/cm.

Figure 5
Scans of the gas gain across the region of plate #202 containing the beam location (X=300mm) before and after exposure to 40mC/cm.

Figure 6
A bidimensional plot of the relative gain of plate #202 (after/before) around the irradiated spot (figure 5) showing the peak at the beam locus. Contour values are in %.

Figure 7
A scan of the FWHM of the xray pulse height peak across the irradiated region of plate #202 (beam at X=300).

Figure 8
The response of the gain of plate #206 (S8900 glass - Au/Ni processing) to intense irradiation.

Figure 9
The data of figure 8 plotted against the logarithm of the charge dose. The gain change settles into logarithmic decline.

Figure 10
A scan of the gain (normalised to that before exposure) across the irradiated area after a charge dose of 46mC/cm. (plate #206)

Figure 11
The gain of plate #206 at the beam location calculated as a fraction of the gain at the edge of the scan region (assumed to be unaffected by the irradiation) so that P/T effects are automatically compensated. (Compare with the data of figure 9)

Figure 12
The FWHM of the xray pulse height distribution measured at the irradiation site on plate #206 as a function of the charge dose.

Figure 13
The transient gain shifts observed on plate #206 when the 300kHz/mm^2 beam is removed at the end of the long exposure and when it is applied to a fresh area of the detector.

Figure 14
A comparison of the response of the gains of plate #206 (S8900 - Au/Ni) and #207 (S8900 - Al) to irradiation in an atmosphere of argon/DME.

Figure 15
A comparison of the gain response of plates #206 and #207 to irradiation in an atmosphere of CF4/DME.

Figure 16
Photo-micrograph of the surface of plate #206 in the region of the beam spot (after 46mC/cm of charge dose). The scale is given by the electrode structure (300μm pattern repeat).

Figure 17
A close-up photograph of the anode-cathode region in the centre of the beam spot (plate #206 after irradiation) showing the difference in deposit density on the cathode and anode.

Figure 18
A highly magnified image (x100) of the deposit on the glass adjacent to the cathode edge in the centre of the irradiated beam spot (plate #206).

FIGURE 1

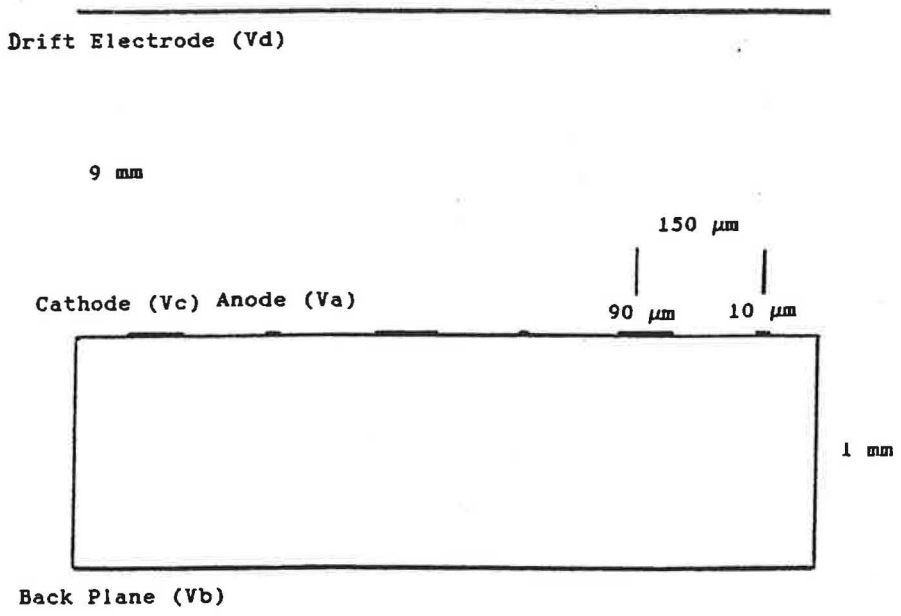
Drift Electrode (Vd)
9 mm
150 μm
Cathode (Vc) Anode (Va)
90 μm
10 μm
1 mm
Back Plane (Vb)

Figure 2a

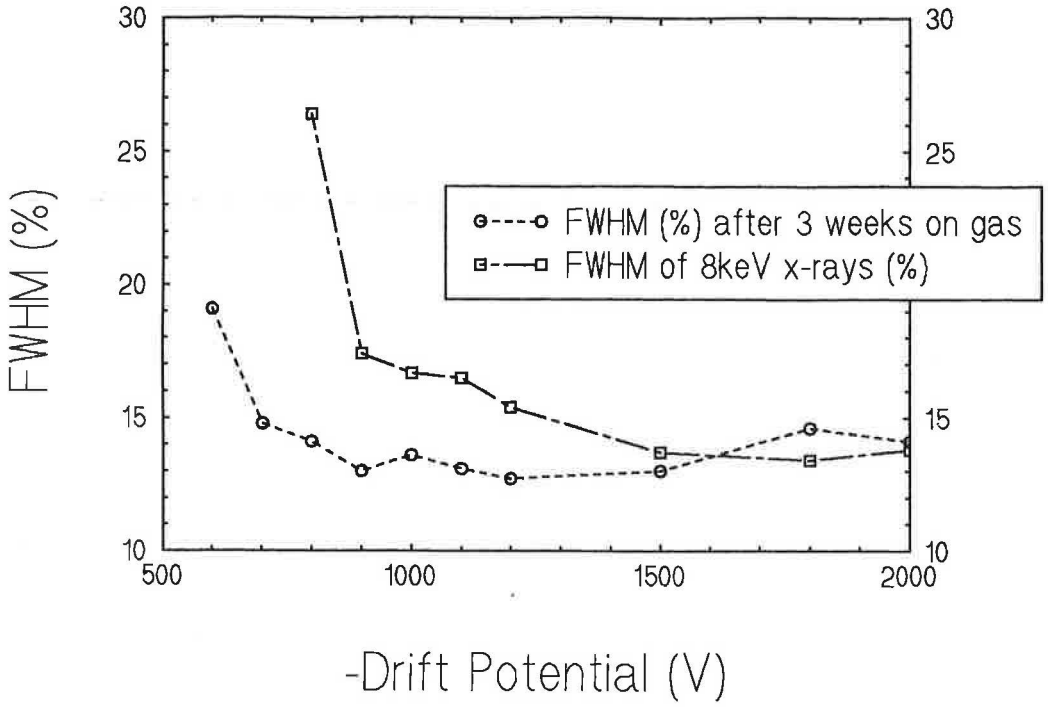

Figure 2b

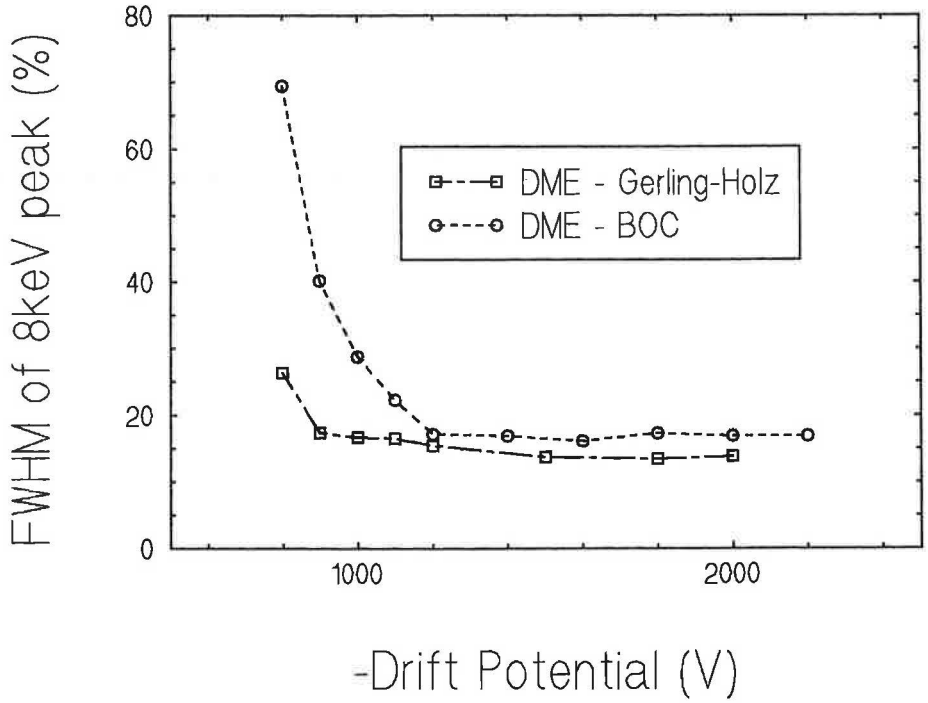

Figure 3

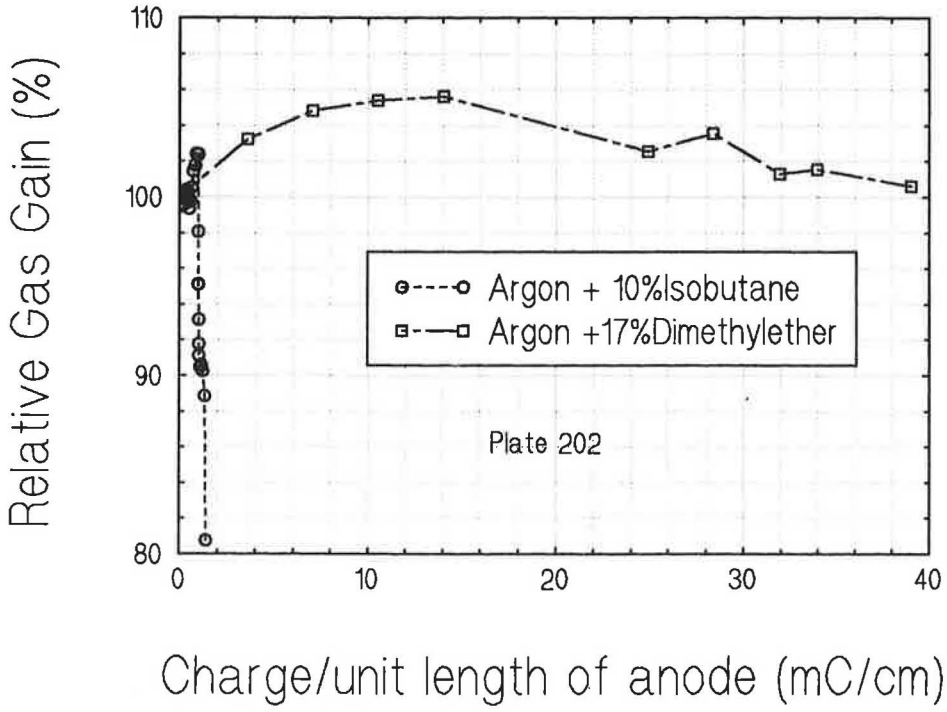

Figure 4

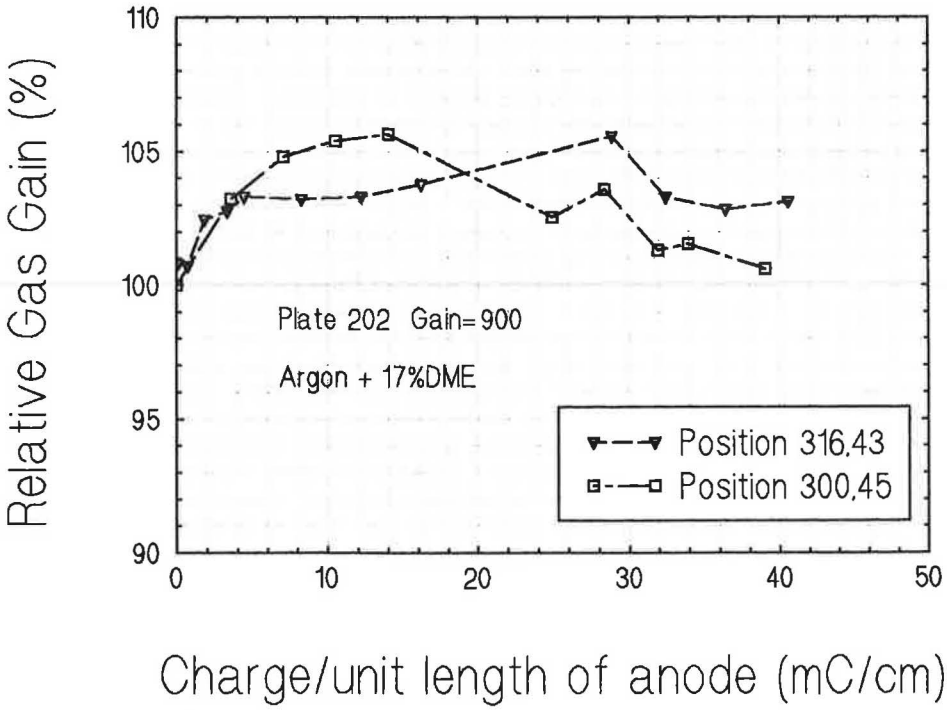

Figure 5

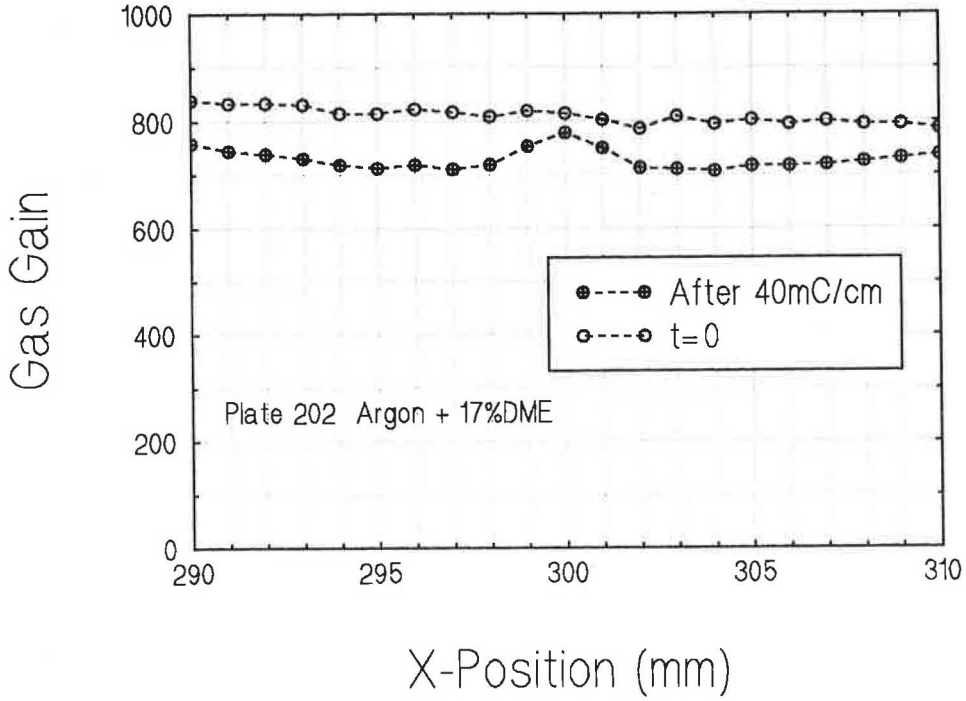

Figure 6

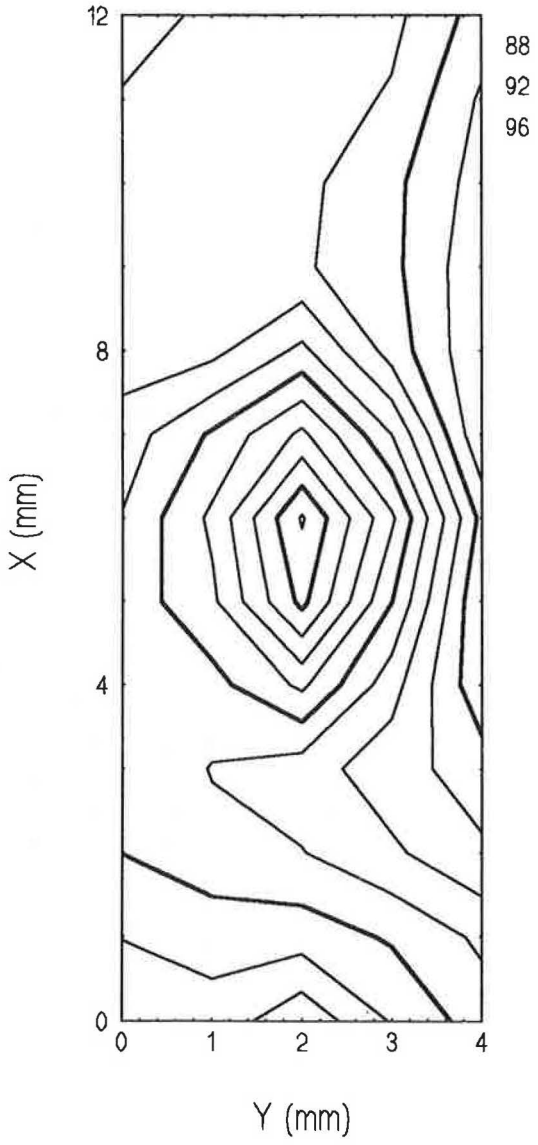

Figure 7

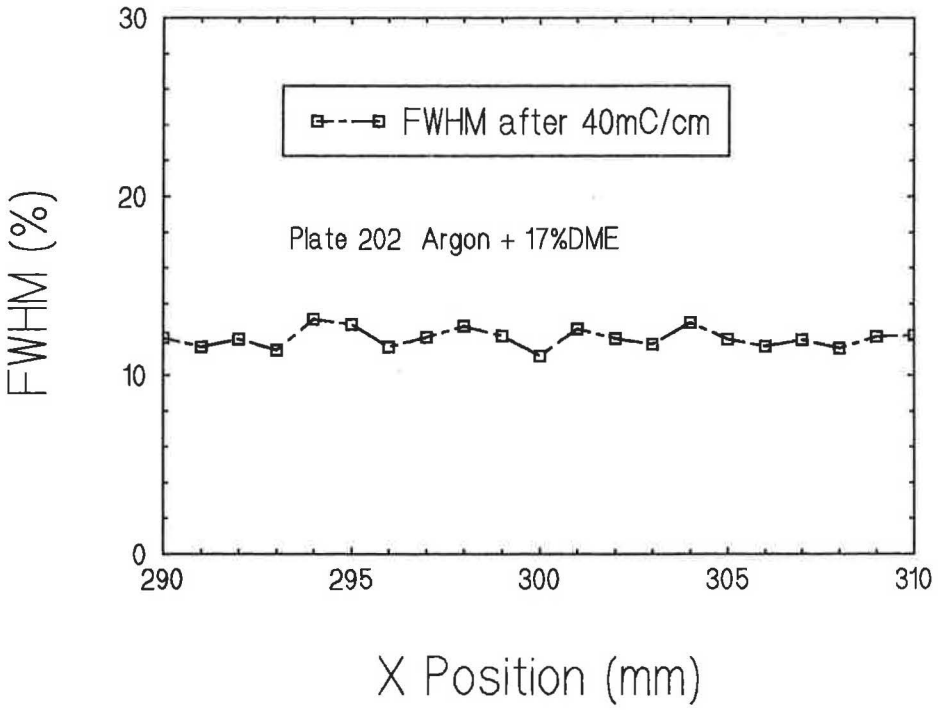
30
20
10
0
290
295
300
305
310
FWHM (%)
FWHM after 40mC/cm
Plate 202 Argon + 17%DME
X Position (mm)

Figure 8

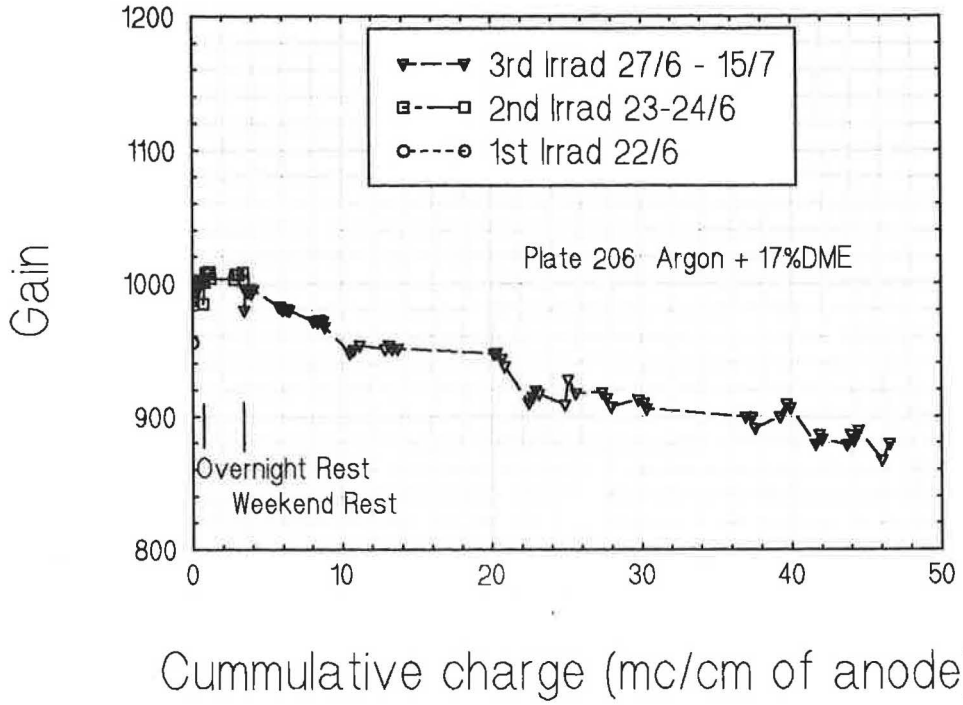

Figure 9

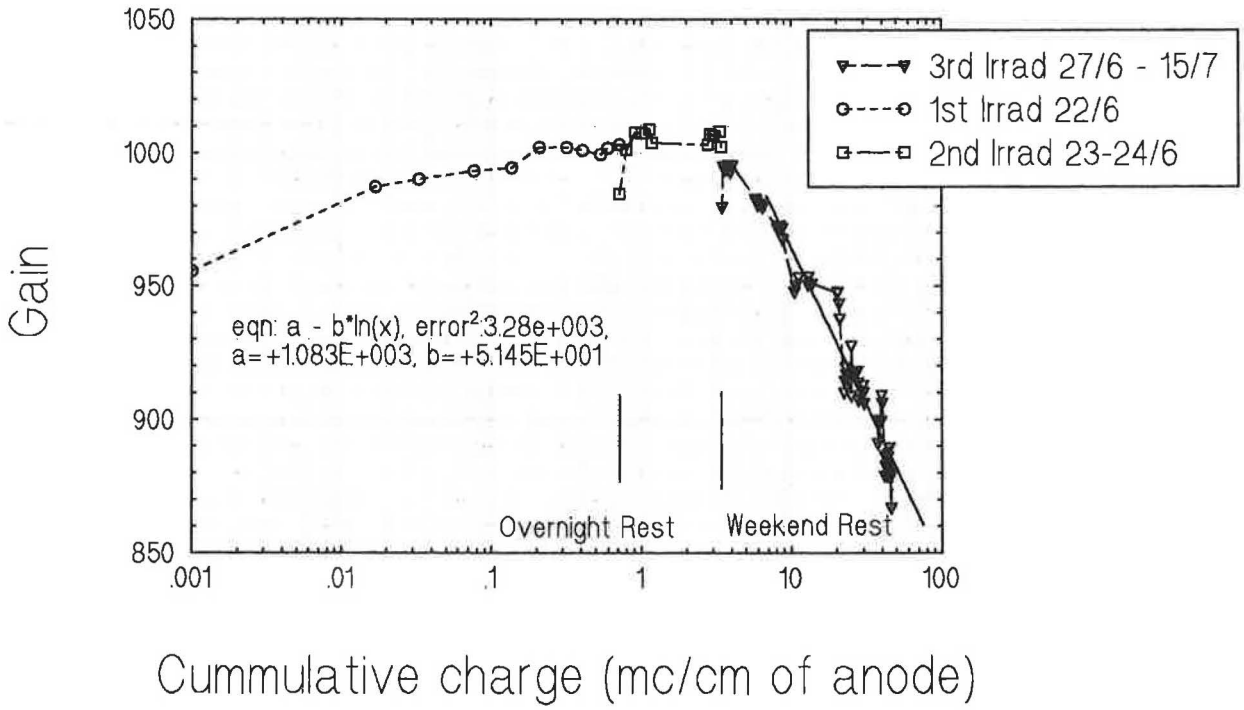

Figure 10

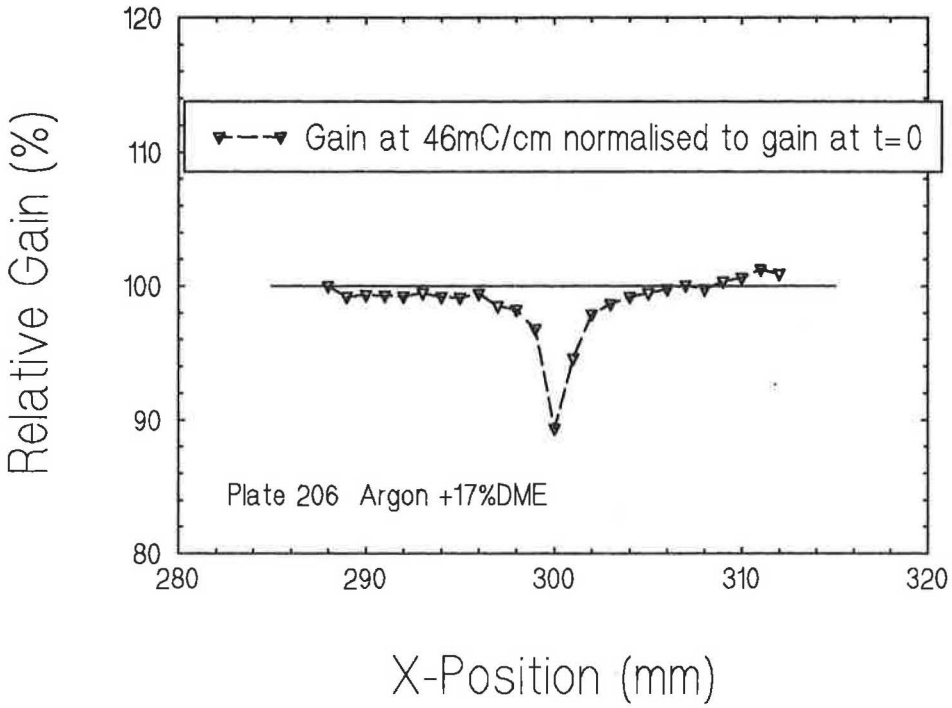

Figure 11

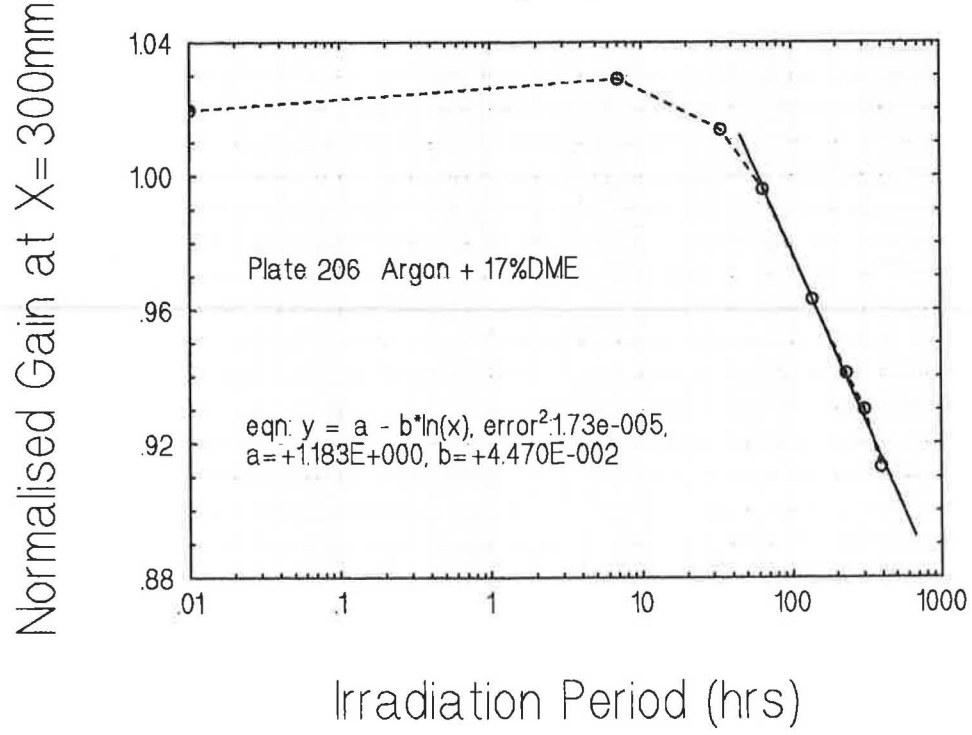

Figure 12

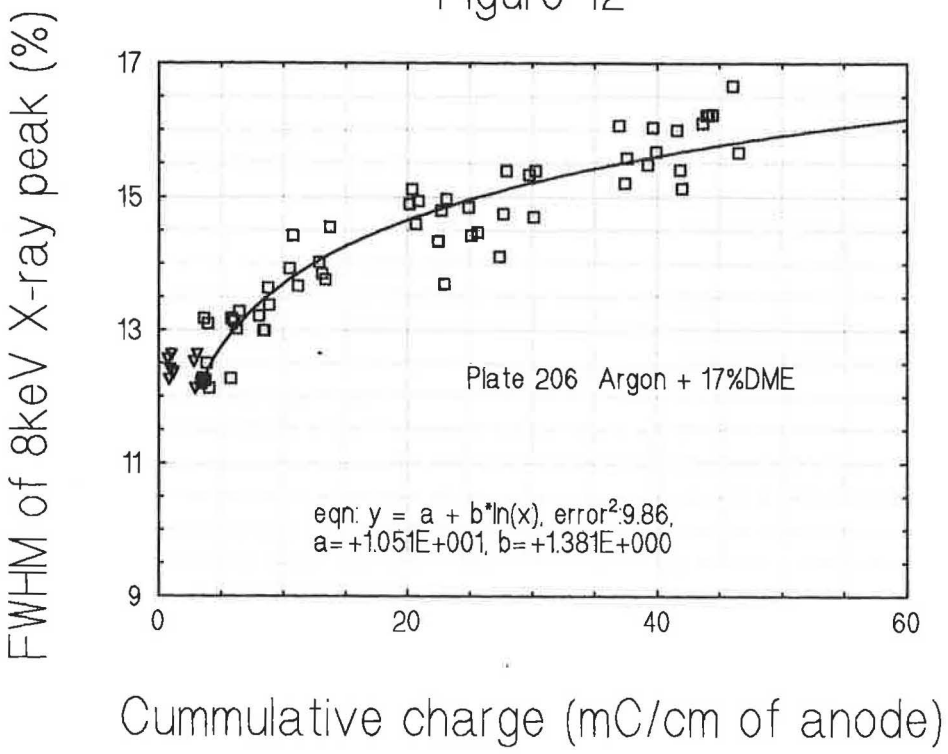

Figure 13

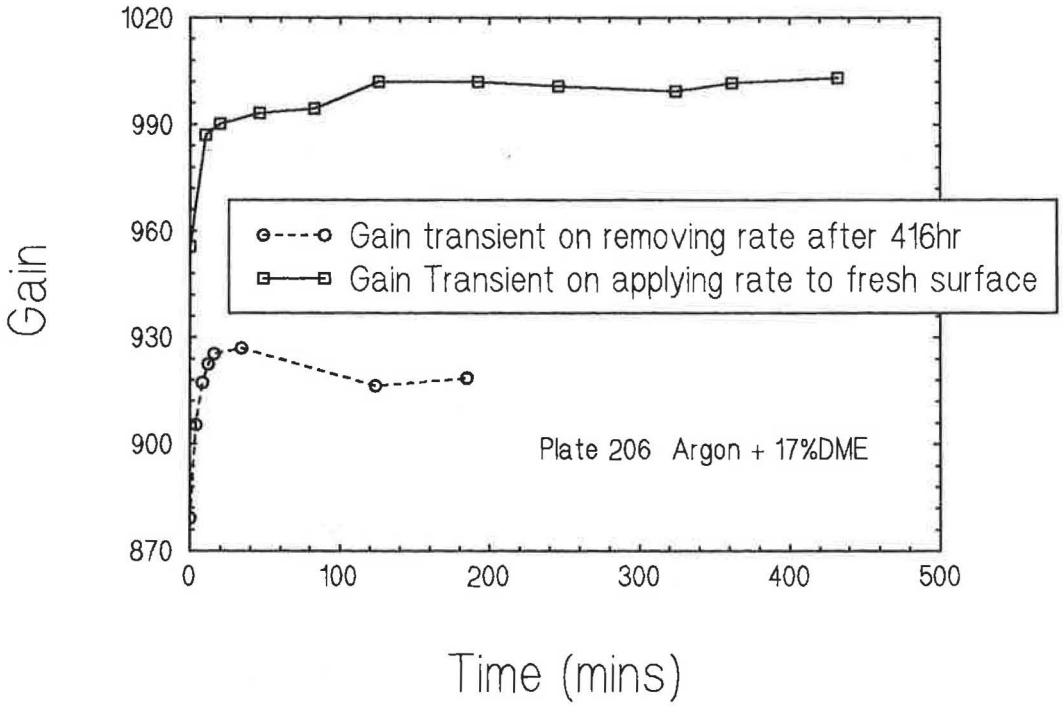

Figure 14

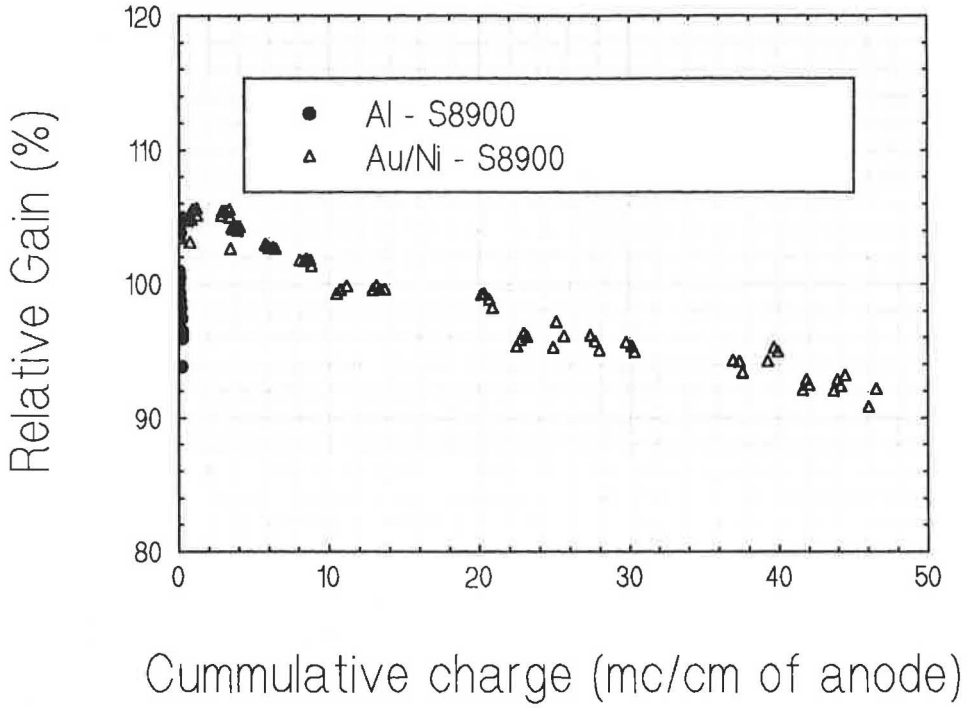

Figure 15

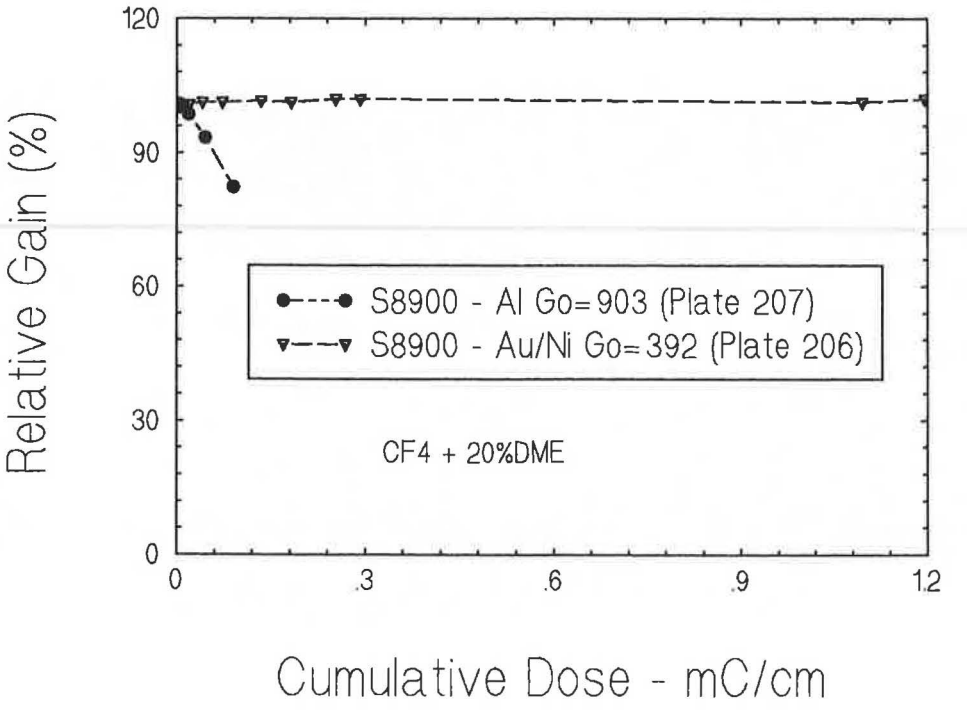

Figure 16

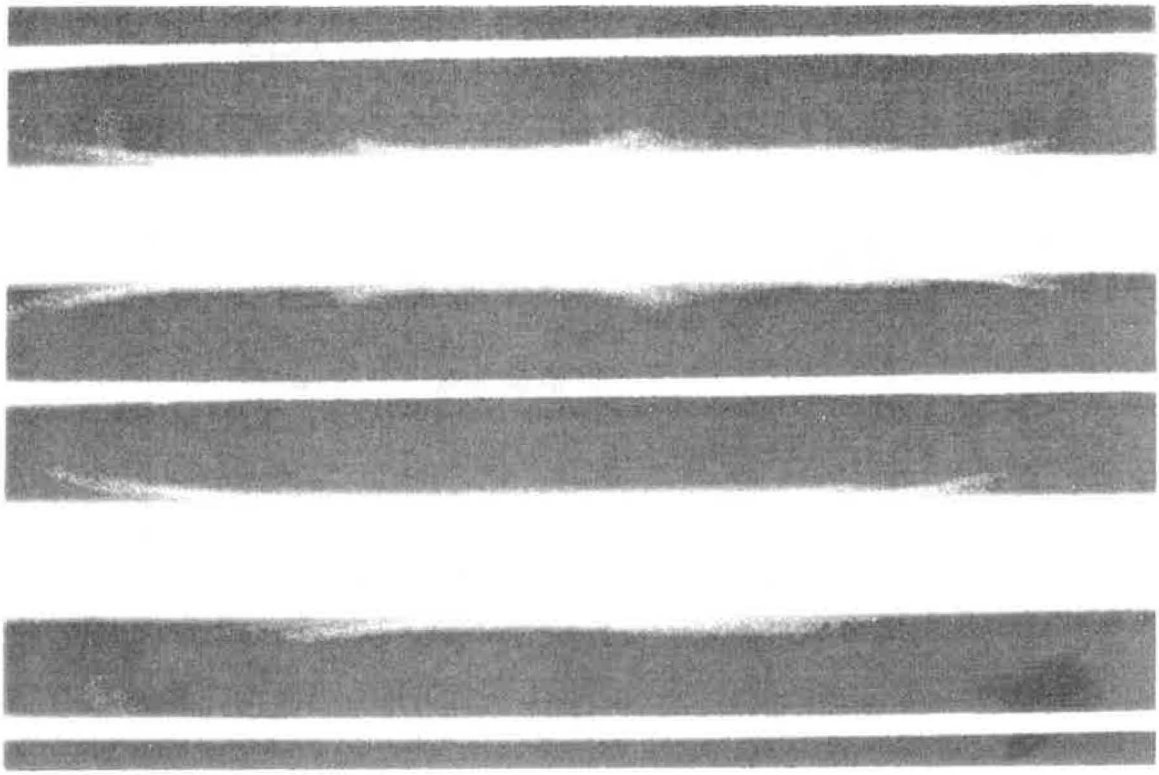

Figure 17

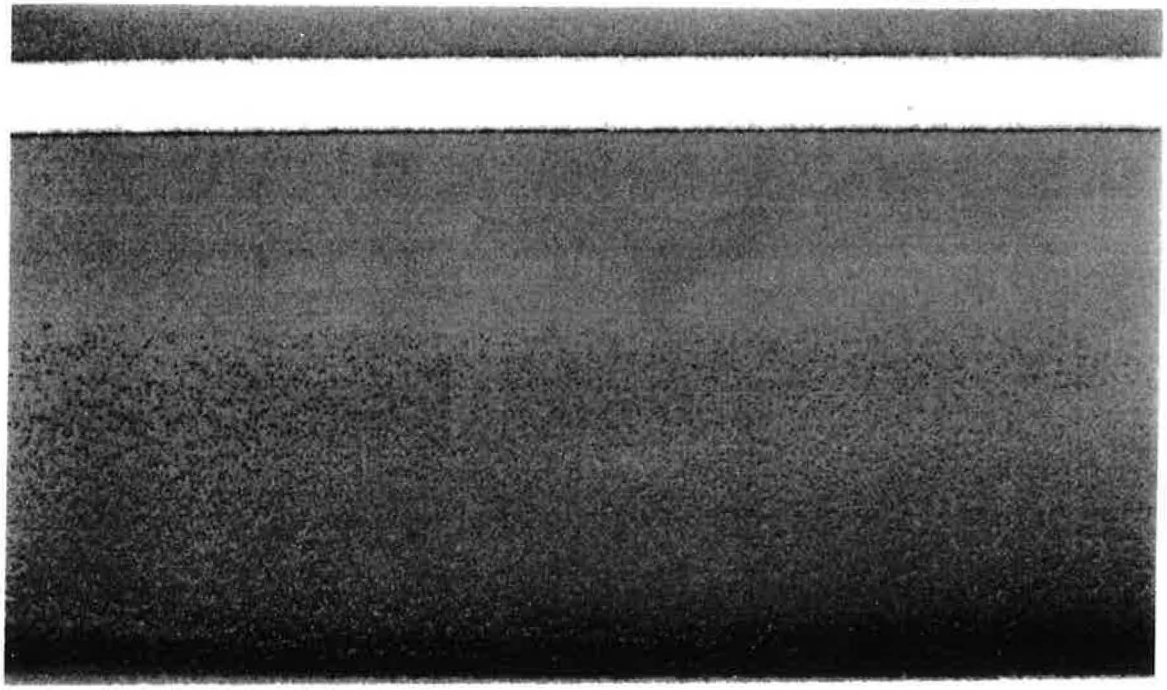

Figure 18